

Imaging Nanometer Phonon Softening at Crystal Surface Steps with 4D Ultrafast Electron Microscopy

Yichao Zhang and David J. Flannigan*



Cite This: *Nano Lett.* 2021, 21, 7332–7338



Read Online

ACCESS |



Metrics & More



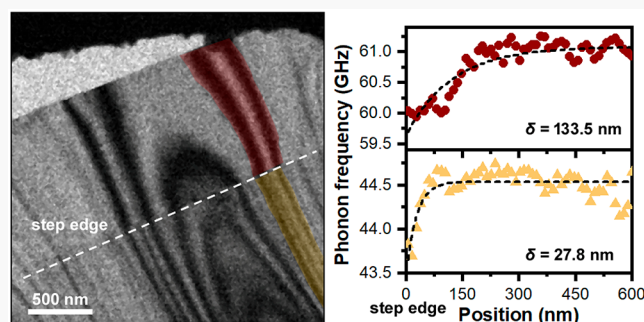
Article Recommendations



Supporting Information

ABSTRACT: Step edges are an important and prevalent topological feature that influence catalytic, electronic, vibrational, and structural properties arising from modulation of atomic-scale force fields due to edge-atom relaxation. Direct probing of ultrafast atomic-to-nanoscale lattice dynamics at individual steps poses a particularly significant challenge owing to demanding spatiotemporal resolution requirements. Here, we achieve such resolutions with femtosecond 4D ultrafast electron microscopy and directly image nanometer-variant softening of photoexcited phonons at individual surface steps. We find large degrees of softening precisely at the step position, with a thickness-dependent, strain-induced frequency modulation extending tens of nanometers laterally from the atomic-scale discontinuity. The effect originates from anisotropic bond dilation and photoinduced incoherent atomic displacements delineated by abrupt molecular-layer cessation. The magnitude and spatiotemporal extent of softening is quantitatively described with a finite-element transient-deformation model. The high spatiotemporal resolutions demonstrated here enable uncovering of new insights into atomic-scale structure–function relationships of highly defect-sensitive, functional materials.

KEYWORDS: transition metal dichalcogenides, MoS_2 , structural dynamics, coherent acoustic phonons, femtosecond photoexcitation, *in situ* TEM



Atomic and molecular arrangements at crystal step edges are such that local catalytic, electronic, vibrational, and structural properties are strongly impacted.^{1–4} Abrupt termination of the lattice at stepped surfaces induces spatially varying interatomic potentials,^{5,6} the precise nature of which depends upon local atomic coordination.^{7,8} Consequently, nanostructured materials properties are strongly modulated in the vicinity of steps, often producing enhanced reactivity and distinct dynamic responses. While the coordination environment has been directly imaged using high-resolution transmission electron microscopy (TEM), associated temporal resolutions are limited to milliseconds.⁹ Importantly, electronic and atomic responses central to emergent behavior originate from picometer-scale excitations that occur on attosecond to picosecond (ps) time scales, the temporal aspects of which are thus amenable to study with ultrafast pump–probe spectroscopic methods.¹⁰ However, even with super-resolution all-optical imaging methods,¹¹ obtaining full spatiotemporal information can be challenging owing to method-insensitivity to dark structures and states.¹² This suggests an opportunity to generate a comprehensive picture of atomic-to-nanoscale dynamics at individual surface steps via the development and application of ultrafast high-resolution imaging methods sensitive to picometer-scale transient responses.

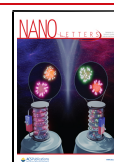
Step-induced phonon nucleation and propagation have been directly imaged with nanometer-femtosecond resolution using

4D ultrafast electron microscopy (UEM).¹³ Because coherent motions are sensitive to nanoscale morphology and atomic coordination,^{14–16} spatiotemporal mapping of vibrational dynamics can be used to probe local responses at individual defects. Owing to the sensitivity of electronic and optical properties of crystalline materials to strain,¹⁷ spatially varying bond modulation due to lattice steps may induce locally distinct behaviors. For example, abrupt changes in planar layer number may produce a spatially varying reduction in vibrational frequency (i.e., phonon softening) due to ultrafast dephasing of oscillatory modes excited perpendicular to the lattice planes.¹⁸ Importantly, while reduced bond strengths at individual step edges have been observed in graphite,¹⁹ no such behavior has been seen in the structurally related and technologically important transition metal dichalcogenides (TMDs), and nothing is yet known about the atomic-to-nanoscale spatial extent of lattice vibrational softening. Here, with high-resolution 4D UEM we spatiotemporally map

Received: June 29, 2021

Revised: August 6, 2021

Published: August 18, 2021



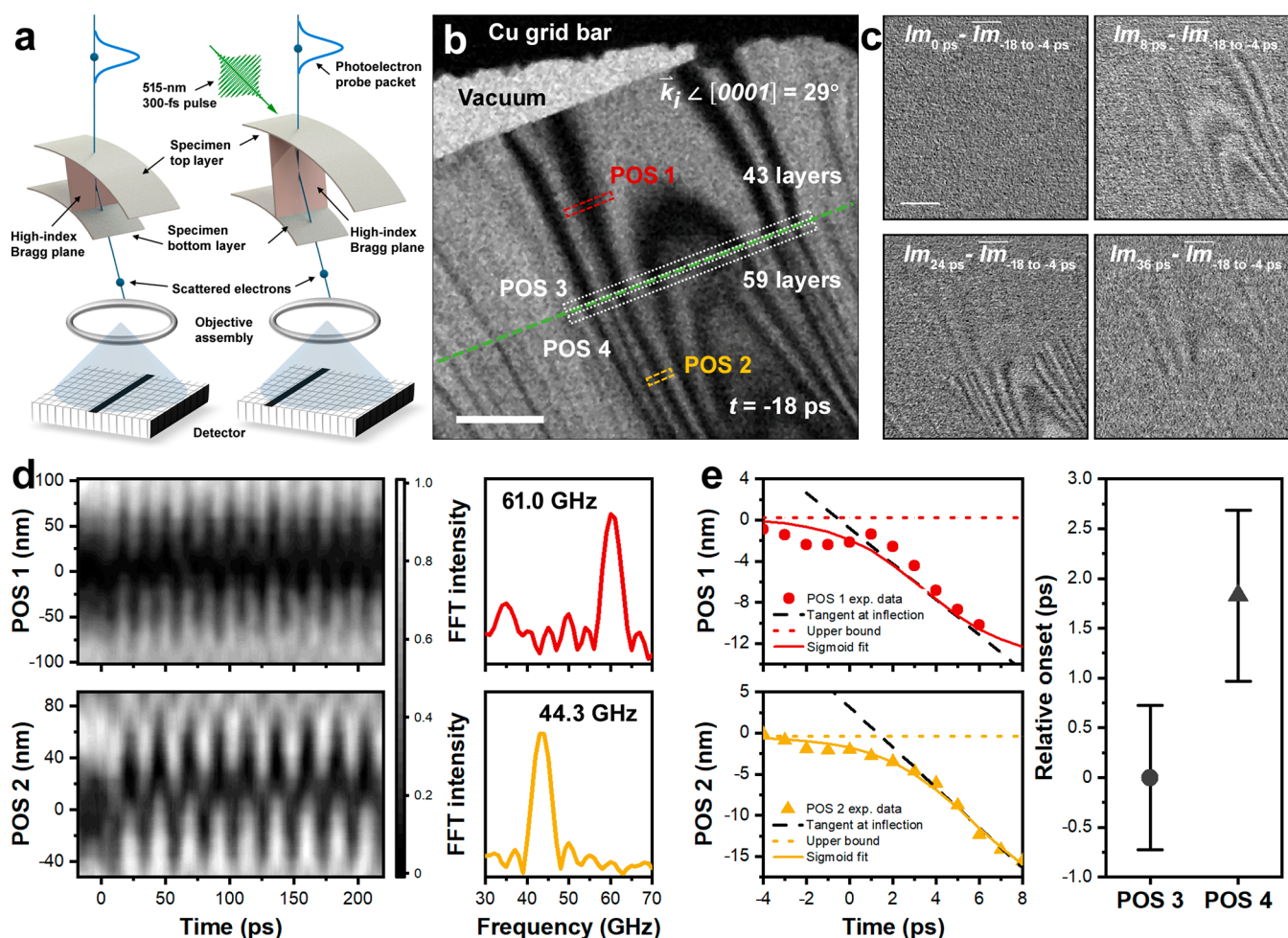


Figure 1. 4D UEM imaging of S–Mo–S interlayer phonon dynamics at a $2H$ - MoS_2 surface step. (a) UEM configuration for ultrafast electron imaging. Ultrashort 200 keV photoelectron probe packets were used to capture snapshots of dynamics following *in situ* 300 fs photoexcitation. Dynamics manifest as coherent contrast oscillations in the image plane when compared to the ground state (i.e., configuration on the left). Tilting of the specimen c -axis away from the photoelectron k_i exposes high-index Bragg planes supporting interlayer dynamics that are then projected onto the detector. (b) Representative UEM image of a stepped surface (green dashed line) on a freestanding flake acquired 18 ps prior to photoexcitation. The $[0001]$ direction is oriented 29° with respect to k_i . The number of layers on either side of the step was determined using measured phonon frequencies and the speed of sound. Error is ± 1 layer. The STCPs in (d) were generated from POS 1 and 2. Contrast dynamics at the step were monitored in POS 3 and 4 (white dotted rectangles). Scale bar = 500 nm. (c) Difference images ($\overline{I_{m_n}} - \overline{I_{m_{n<0}}}$) at select times n showing phonon dephasing caused by the step ($\overline{I_{m_{n<0}}} = \text{average of pretime-zero images}$). Scale bar = 500 nm. (d) STCPs and corresponding FFTs of POS 1 and 2. Color bar represents normalized counts. (e) Relative onset of ultrafast photoinduced phonon dynamics in POS 1 and 2. Error bars are 1 std dev from the average of all bend contours in POS 3 and 4.

nanometer coherent phonon vibrational frequencies at individual surface steps in ultrathin crystals of the TMD archetype, $2H$ - MoS_2 , and discover spatially varying, thickness-dependent anisotropic softening. Using the highly sensitive fs electron imaging capabilities unique to UEM,^{20–22} we directly probed the associated picometer-scale lattice deformations seeded at individual surface steps, and we quantified nanometer phonon-vibrational responses in space and time.

Figure 1 shows the 4D UEM configuration used to directly image coherent phonon dynamics at individual surface steps on ultrathin $2H$ - MoS_2 crystals. Here, a single flake was oriented in such a way with respect to the incident electron wave vector, k_i , that lattice oscillations photoexcited along the crystallographic c -axis layer-stacking direction were isolated (Figure 1a,b).^{15,18} Picometer lattice distortions traveling between the outer layers produce characteristic nonpropagating contrast oscillations, as opposed to traveling basal-plane modes.^{13,23} A spatially gradual curvature of the flake produces

distinct, symmetric bend contours, the 2D projected positions of which are extremely sensitive to local phonon-induced lattice deformations and associated oscillations of the local Bragg-scattering condition (Figure 1c).²⁴ Accordingly, ultrafast photoinduced phonon responses can be spatiotemporally mapped by selecting positions of interest (POS) and collapsing to one spatial dimension in the time domain to generate a space–time contour plot (STCP; Figure 1d).^{14,25}

Differences in the number of S–Mo–S layers delineated by the surface step cause dramatic variations in c -axis phonon frequencies.¹⁸ This can be readily seen in a UEM difference-image series and in the oscillatory frequency of portions of bend contours spanning the step (Figure 1c,d). Here, a difference of 16 S–Mo–S layers produces two distinct vibrational responses of 61.0 and 44.3 GHz approximately 500 nm from the step in the 43-layer and 59-layer regions, respectively. The responses arise from fs photoexcitation and propagation of coherent acoustic phonons back and forth

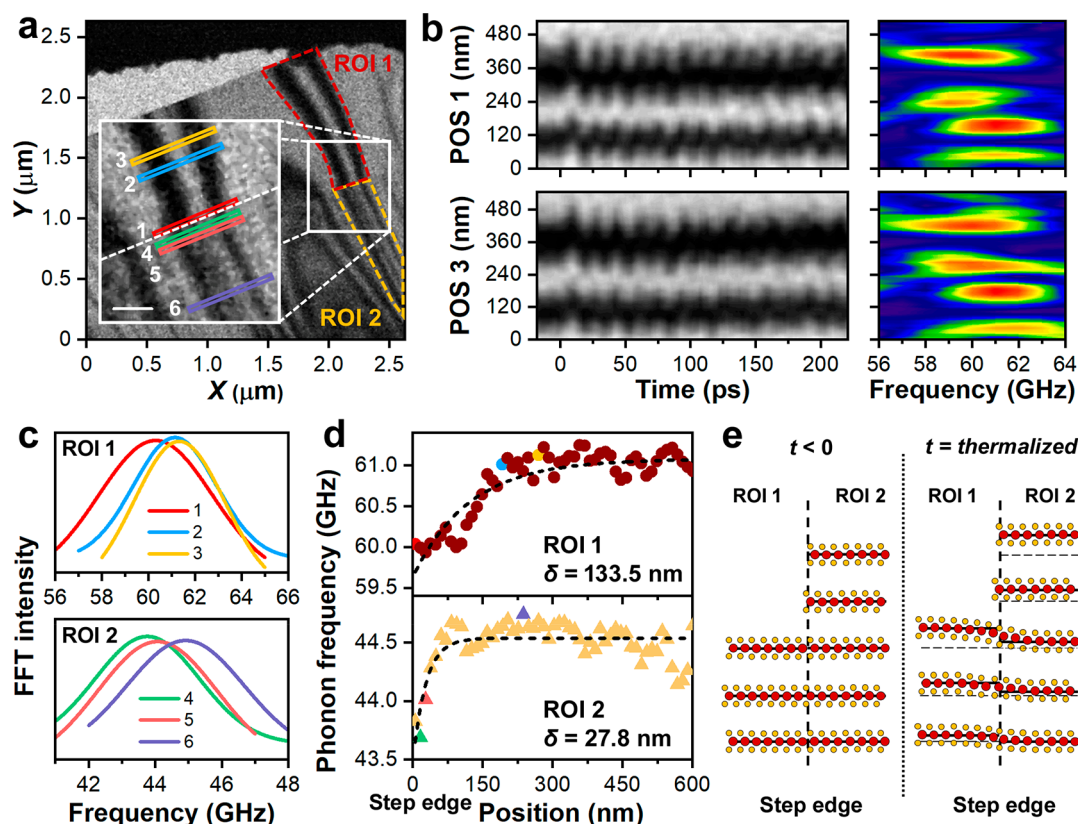


Figure 2. Ultrafast nanoscale mapping of spatially variant phonon softening at a surface step. (a) Representative UEM image of a freestanding 2H-MoS₂ flake with highlighted ROIs from which phonon dynamics were mapped. Each ROI contains a symmetric bend contour along which ps phonon dynamics were quantified at 11 nm steps. Expanded view highlights select positions at which phonon frequencies were quantified in the vicinity of the step (white dashed line). Scale bar = 150 nm. (b) STCPs of positions (POS) 1 and 3 in panel (a) and corresponding spatially dependent FFTs from which average phonon frequency was determined. (c) FFTs of select positions in panel (a) from which blue shifts in average phonon frequency moving away from the step were determined. (d) Position-dependent phonon frequency in each ROI. Position is relative to the step, which is set to 0 nm. Spatially varying softening extends away from the step following eq 1 (dashed-line fits) before plateauing to spatially invariant single oscillatory values (see Figure 1d). (e) Illustration of the atomic-level origins of softening at a step. The $t < 0$ panel is the idealized prephotoexcitation ground-state structure used as a reference, while the $t = \text{thermalized}$ panel is postphotoexcitation at initial system thermalization. Vertical dashed lines along the layer-stacking direction represent the step position. Horizontal dashed (solid) lines in the $t = \text{thermalized}$ panel mark the initial (expanded) layer positions. Anisotropic expansion along the stacking axis is especially evident in ROI 2, as is bending of the shared S–Mo–S layers near the step.

along the layer-stacking direction, with a path-length difference of 10.4 nm for the regions delineated by the step. (Thicknesses and number of layers were determined using the C_{33} elastic constant for 2H-MoS₂ and the measured vibrational frequencies.²⁶) Following fs photoexcitation, the interlayer modes rapidly become out of phase with one another, triggered by a 1.8 ps delay between the initial local lattice responses (Figure 1e; also see the Supporting Information). Interlayer-mode excitation originates from modulation of the c -axis unit-cell parameter driven by charge-carrier excitation, electron–phonon coupling, and subsequent system thermalization.^{18,27} The 1.8 ps delay falls within the range of electron–phonon coupling dictated by number of layers, crystal boundary conditions, and defect density, thus suggesting a thickness-dependent carrier- and lattice-relaxation response^{28,29} convoluted with electronic-state modulation at the step.³⁰

As shown in Figure 2, nanometer ultrafast spatiotemporal mapping with 4D UEM of phonon vibrational frequencies at a discrete surface step reveals a thickness-dependent, spatially varying softening of the oscillatory responses extending tens to hundreds of nanometers away from the atomic-scale defect. Here, phonon frequencies extending away from the step into

either region of interest (ROI) exhibit an increase of up to 1.5 GHz before plateauing to intrinsic, defect-free vibrational responses (Figure 2a–d). Though the precise functional form of spatially varying softening has not previously been resolved for layered materials, density functional theory calculations predict an exponential decay of step-induced interplanar relaxation with increasing distance in structurally isotropic Cu.³¹ Accordingly, the functional form of such step-modulated bonding interactions when considered in the frequency domain will display an upward exponential decay indicative of an increase in bond stiffness (eq 1).

$$f(d) = f_{d \rightarrow \infty} - Ae^{-d/\delta} \quad (1)$$

Here, d is the distance from the step, $f_{d \rightarrow \infty}$ is the frequency far from the step, A is the magnitude of the frequency change (i.e., $A = f_{d \rightarrow \infty} - f_{d=0}$), and δ is the spatial constant. Fitting of the spatially varying phonon softening in ROIs 1 and 2 with eq 1 returns a significant reduction in the C_{33} elastic constant of 2.6 GPa, which is 5% of the intrinsic value for pristine 2H-MoS₂.²⁶ This reduction is nearly a factor of 2 larger than that at lattice-substrate edges for monolayer MoS₂,³² and it is an order of magnitude larger than that seen for graphene steps in highly

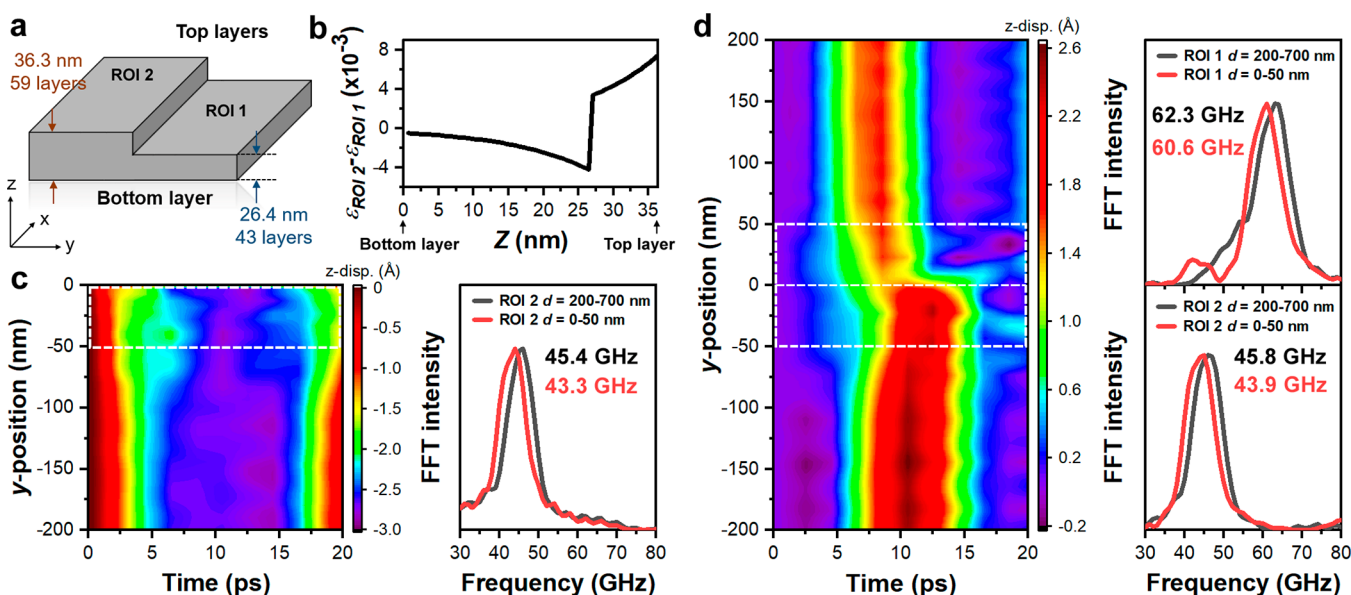


Figure 3. Step-dependent nanometer phonon vibrational dynamics. (a) Model structure of the stepped surface. Layer numbers, thicknesses, and positions for each ROI were constructed to closely match the specimen highlighted in Figures 1 and 2. For reference, the pump-laser excitation is incident at the top layers. (b) Varying photoinduced *c*-axis strain (ϵ) derived from distinct anisotropic photothermal expansions in each ROI in the vicinity of a plane parallel to the *z*-direction that defines the position of the step (see Figure 2e). The discontinuity in $\Delta\epsilon$ at 26.4 nm occurs at the transition from the final shared layer (i.e., top layer of ROI 1) to the first shared layer in ROI 2, while the behaviors follow the depth-dependent optical absorption profiles away from this transition region. The “Top-layer” label on the *x*-axis at 36.3 nm corresponds to the top layer of ROI 2. Simulated STCPs of the top (c) and bottom (d) layers, along with the $d = 200\text{--}700$ nm (i.e., far from the step) and $d = 0\text{--}50$ nm (i.e., near the step) normalized FFTs, for ROIs 1 and 2 spanning the first 20 ps following thermalization at $t = 0$ ps. Note the STCP in panel c only shows ROI 2 because no shared layer exists. Color bar represents *z*-displacement (i.e., parallel to the *c*-axis) in Å. The step is positioned at 0 nm.

ordered pyrolytic graphite.¹⁹ This suggests an atomic-scale compositional sensitivity, where the degree of disruption of collective bonding interactions varies with interlayer sliding and precise orbital overlap, as seen for layer twisting.³³ The high sensitivity of 4D UEM imaging is such that differences in δ for each region can be resolved; here, δ is nearly five times smaller in the thicker ROI 2 ($\delta_{\text{ROI 2}} = 27.8$ nm; $A = 1.2$ GHz) than in ROI 1 ($\delta_{\text{ROI 1}} = 133.5$ nm; $A = 1.5$ GHz) (Figure 2d). This is due to enhanced stiffness induced by the additional 16 S–Mo–S layers, resulting in additional collective bonding within the thicker region.³⁴

The observed localized bond-stiffness reduction at a surface step is associated with a bending of the basal plane along the layer stacking direction (Figure 2e), which is expected to be rapidly damped spatially for multilayer crystals relative to monolayer flakes.^{32,34} This is due to an overall increase in stiffness as layers are added and collective bonding increases, thus producing an associated increase in the relevant elastic constant. In light of this, the origin of spatially varying softening of interlayer phonon modes in the vicinity of a surface step in layered materials has two distinct contributing factors. First, the precise responses of coherent acoustic phonons are extremely sensitive to local structural properties such that a reduction in bond stiffness in the propagation direction at a step will directly result in an associated softening of the vibrational frequency.^{6,14,18} The force field near a crystal step also depends on the crystallographic plane that is cleaved to form the edge, thus giving rise to a multicomponent field map encompassing edge, corner, and terrace atoms.³⁵ This particular softening mechanism can occur with and without external perturbation (e.g., fs photoexcitation).

The second factor is perturbation-dependent and involves an initial ultrafast anisotropic expansion along the layer stacking

direction (Figure 2e). A discontinuous response in the photoinduced interlayer expansion at the spatial transition from shared to unshared layers triggers ps dephasing of *c*-axis phonon modes at the step.^{15,18} This arises from a variable *c*-axis displacement of each layer (e.g., S–Mo–S layers for MoS₂) in shared basal planes spanning the step owing to differing photon-absorption profiles (see the Supporting Information). To compensate for this tortured configuration, the layers undergo additional bending in the direction parallel to the [0001] direction in the vicinity of the step. This imposes an in-plane tensile strain via elongation of basal-plane covalent bonds, which then induces an interlayer shearing motion and slipping of the planes.^{36,37} This further produces a reduction of the C_{33} elastic constant and an associated lattice vibrational softening near the step. Layer deformation gradually declines spatially with distance away from the step, and the stiffness displays a thickness-dependent upward exponential decay as the defect-free, blue-shifted vibrational frequency is approached.

Finite-element transient-deformation analysis was performed on a model stepped surface and compared to the 4D UEM imaging results (Figure 3; see the Supporting Information). The model structure consisted of two regions, each with approximately the same thickness as ROIs 1 and 2 and separated by a 9.9 nm high step (Figure 3a). At $t = 0$ ps, the structure is under a laterally uniform *c*-axis-varying tensile strain. This is meant to simulate coherent fs photoexcitation and subsequent ultrafast photothermal lattice expansion (i.e., $t = \text{thermalized}$). Thus, $t = 0$ ps in the model represents the initial moment of complete lattice thermalization (i.e., initial full interlayer expansion). This is a subtle but important distinction from the experimental onset of ultrafast photoinduced dynamics, which encompasses the initial fs-to-ps

thermalization process, as well as subsequent full initial photothermal lattice expansion and onset of coherent oscillatory motion.

The first moment of full interlayer expansion is immediately followed by a few-ps, Å-scale contraction along the *z*-direction as the system relaxes via coherent phonon excitation (Figure 3c,d). Experimentally observed ps phonon dephasing¹⁸ is expected to manifest here as well. Because all layers of ROI 1 are shared with ROI 2, the optical-absorption profile along the layer-stacking direction differs in each region and produces an initial anisotropic modulation of bond lengths through the crystal depth arising from an ultrafast lateral carrier-density and electron–phonon coupling discontinuity at the step (see the Supporting Information). This manifests as a discontinuous difference–strain profile, as shown in Figure 3b. The initial Å-ps contraction is unrelated to dominant ultrafast *c*-axis contraction in TMDs for absorbed fluences below 1 mJ/cm² and above-gap photon energies, which is instead driven by modulation of interlayer bonding interactions.²⁷

The finite-element transient-deformation model captures both the thickness-dependent phonon softening in the vicinity of the step and the spatially varying frequency blue shift moving away from the defect (Figure 3c,d). Further, the magnitude of softening in both ROIs (i.e., the *A* parameter in eq 1) agrees well with experiment. Note that because an instantaneous strain is simultaneously applied to both ROIs, the experimentally observed relative delay in the onset of dynamics (Figure 1e and Supporting Information), which also emerges in the model (Figure 3d), is itself not the main cause of softening. Though softening due to the step is not incorporated into the model (the same elastic constants were applied to the entire structure), a spatially varying blue shift in phonon frequency is still seen in both ROIs. This supports the hypothesis that ps dephasing of *c*-axis phonons due to local bond-strength variation on either side of the step is the main source of softening. Slightly elevated values of the modeled phonon frequencies far from the step, as compared to experiment, arise from differences between element and layer thickness.³⁸ Additional slight discrepancies arise from general photothermal softening of materials; tensile strains arising from pulsed-laser excitation and subsequent equilibration at elevated temperatures soften phonon vibrational modes due to weakened bonding.^{39,40} Such an effect was not incorporated into the model, as relative variations in local vibrational responses were the focus.

In summary, our results show that ultrafast photoinduced coherent-phonon dephasing causes an atomic-to-nanoscale thickness-dependent spatial variation in softening of vibrational modes at crystal surface steps. This finding was enabled by the highly sensitive, high-resolution ultrafast real-space electron-imaging capabilities unique to 4D UEM, with which discrete nanometer phonon responses precisely at individual steps were elucidated and quantified. The spatially modulated optovibrational response arising from structurally directed photoperturbation reveals the molecular-level origins of step-induced phonon softening, with potential impacts on defect-sensitive and strain-tunable optical and electronic materials. The picometer-sensitive ultrafast electron-imaging approach demonstrated here is broadly applicable to a wide range of materials and is especially capable of elucidating discrete atomic-to-nanoscale heterogeneous effects that influence overall material functionality.

METHODS

Ultrafast, High-Resolution *In Situ* Optical Pump/Electron-Probe Imaging. Ultrafast electron imaging experiments were conducted with a 200 kV UEM (FEI Tecnai Femto, Thermo Fisher Scientific) equipped with a 100 μm truncated and graphite-encircled LaB₆ source (Applied Physics Technologies) set 350 μm back from a custom 1 mm Wehnelt aperture.^{41,42} The specimen was photoexcited (PHAROS, Light Conversion) *in situ* with 515 nm wavelength light, an average absorbed fluence of 1.4 mJ/cm², a 20 kHz repetition rate, a pulse duration of 300 fs (full-width at half-max, fwhm; GECO scanning autocorrelator, Light Conversion), and a spot size of 120 μm (fwhm; measured externally with a Newport 190–1,100 nm Si CCD beam profiler and calculated extrapolation to the specimen position). This produced a nearly flat intensity profile across the approximately 2 μm by 2 μm field of view. The angle of incidence of *in situ* photoexcitation was 4° relative to the photoelectron optical axis, with the 2H-MoS₂ crystal [0001] direction oriented 29° with respect to *k_i* (Figure 1b). Second harmonic (2.4 eV photons) of the fundamental was generated using a harmonics module (HIRO, Light Conversion), while fourth-harmonic light (4.8 eV photons) was generated externally with standard nonlinear optics.

Photoelectrons were generated with fourth-harmonic light and had an estimated pulse duration of 1 ps (fwhm).⁴² Signal for each image was acquired for 30 s, equating to 6 × 10⁵ pump–probe cycles per frame; each photoelectron packet contained an estimated 100 electrons at the detector. Supporting Information, Video 1 consists of 240 individual frames. Thus, the 2H-MoS₂ flake underwent 144 million repeatable pump–probe cycles during this particular experiment. For all UEM images, a 40 μm diameter objective aperture centered on the photoelectron optic axis was used to enhance contrast. Time delays were established using a motorized linear translation stage (Aerotech PRO165LM with Soloist CP10-MXU controller) and a broadband hollow retroreflector (Newport, UBBR2.5–1UV). All ultrafast experiments were performed in a stroboscopic pump–probe manner using randomized 1 ps time steps via automated communication between the translation-stage controller and the UEM camera (Gatan OneView).⁴³

All UEM images were 16 bit and were postprocessed in the same manner. After putting the series in sequential order following randomized acquisition, the Despeckle filter in Fiji^{44,45} was applied to each image in order to effectively remove saturated pixels arising from spurious high-energy particle impact. Next, the Fiji Template Matching plug-in was used to conduct a pixel-by-pixel cross correlation of a select ROI in each image (here, a section of the Cu grid bar) with the same ROI in the first image in the series. The resulting data was then imported into MATLAB, and a custom-written algorithm was used to overlay each image such that slow changes in the field of view (i.e., specimen drift) were corrected. Finally, image contrast was enhanced by setting pixels with counts in the 1st and 99th percentiles to 0 and 65536, respectively, and then rescaling all other pixels to span the same range.

Preparation of Ultrathin, Electron-Transparent 2H-MoS₂ Flakes. Electron-transparent flakes for the UEM measurements were prepared using adhesive tape and repeated mechanical exfoliation of a bulk 2H-MoS₂ crystal (2D

Semiconductors).^{13,38} Isolated flakes were transferred onto a NaCl crystal (Ted Pella) by rubbing the tape on the surface. Coverage and the presence of ultrathin flakes was then qualitatively checked using an optical stereo microscope (AmScope). The NaCl crystal with specimen flakes was then repeatedly washed with isopropyl alcohol to remove adhesive, followed by drying in air. Next, 15 μ L of a 4 wt % solution of poly(methyl methacrylate) (PMMA) in anisole was drop-cast onto the NaCl surface supporting the flakes and then annealed at 100 °C in air for 10 min. The resulting PMMA/specimen film was then floated off the NaCl crystal in deionized water and captured on a 2000 mesh Cu TEM grid (Ted Pella, G2000HS). Finally, the specimen was repeatedly washed with acetone to remove PMMA, salt, and any remaining adhesive.

■ ASSOCIATED CONTENT

Supporting Information


The Supporting Information is available free of charge at <https://pubs.acs.org/doi/10.1021/acs.nanolett.1c02524>.

Additional Materials and Methods describing preliminary TEM structural characterization, nanometer spatial mapping of the onset of fs photoinduced phonon dynamics, details of the nanometer spatial mapping of phonon softening at the step, details of the method for determining crystal thickness in each ROI, calculation of the photoinduced *c*-axis strain profile in the layer-stacking direction of each ROI, and details of the finite-element transient-deformation analysis (PDF)

Video 1: High spatiotemporal-resolution UEM video of phonon dynamics at a step edge in an ultrathin 2H-MoS₂ flake (AVI)

■ AUTHOR INFORMATION

Corresponding Author

David J. Flannigan — Department of Chemical Engineering and Materials Science, University of Minnesota, Minneapolis, Minnesota 55455, United States;  orcid.org/0000-0002-1829-1868; Email: flan0076@umn.edu

Author

Yichao Zhang — Department of Chemical Engineering and Materials Science, University of Minnesota, Minneapolis, Minnesota 55455, United States

Complete contact information is available at:

<https://pubs.acs.org/doi/10.1021/acs.nanolett.1c02524>

Author Contributions

Y.Z. contributed to the formal analysis, investigation, methodology, software, validation, visualization, writing of the original draft, and writing of the review and editing. D.J.F. contributed to the conceptualization, formal analysis, funding acquisition, methodology, project administration, resources, supervision, visualization, writing of the original draft, and writing of the review and editing. See the NISO CRediT taxonomy for definitions of contributor roles.

Notes

The authors declare no competing financial interest.

■ ACKNOWLEDGMENTS

This material is based on work supported by the National Science Foundation under Grant No. DMR-1654318. This work was supported partially by the National Science

Foundation through the University of Minnesota MRSEC under Award Number DMR-2011401. Y.Z. acknowledges support from the Louise T. Dosdall Fellowship.

■ REFERENCES

- (1) Poelsema, B.; Mechttersheimer, G.; Comsa, G. The interaction of hydrogen with platinum(s)-9(111) \times (111) studied with helium beam diffraction. *Surf. Sci.* **1981**, *111*, 519–544.
- (2) Barth, J. V.; Brune, H.; Ertl, G.; Behm, R. J. Scanning tunneling microscopy observations on the reconstructed Au(111) surface: Atomic structure, long-range superstructure, rotational domains, and surface defects. *Phys. Rev. B: Condens. Matter Mater. Phys.* **1990**, *42*, 9307–9318.
- (3) Crommie, M. F.; Lutz, C. P.; Eigler, D. M. Imaging standing waves in a two-dimensional electron gas. *Nature* **1993**, *363*, 524–527.
- (4) Niu, L.; Gaspar, D. J.; Sibener, S. J. Phonons localized at step edges: A route to understanding forces at extended surface defects. *Science* **1995**, *268*, 847–850.
- (5) Ibach, H.; Bruchmann, D. Surface phonons on stepped Pt(111) surfaces. *Phys. Rev. Lett.* **1978**, *41*, 958–960.
- (6) Knipp, P. Phonons on stepped surfaces. *Phys. Rev. B: Condens. Matter Mater. Phys.* **1991**, *43*, 6908–6923.
- (7) Hunley, D. P.; Flynn, T. J.; Dodson, T.; Sundararajan, A.; Boland, M. J.; Strachan, D. R. Friction, adhesion, and elasticity of graphene edges. *Phys. Rev. B: Condens. Matter Mater. Phys.* **2013**, *87*, 035417.
- (8) Durukanoglu, S.; Kara, A.; Rahman, T. S. Local structural and vibrational properties of stepped surfaces: Cu(211), Cu(511), and Cu(331). *Phys. Rev. B: Condens. Matter Mater. Phys.* **1997**, *55*, 13894–13903.
- (9) Liu, Z.; Lin, Y.-C.; Lu, C.-C.; Yeh, C.-H.; Chiu, P.-W.; Iijima, S.; Suenaga, K. *In situ* observation of step-edge in-plane growth of graphene in a STEM. *Nat. Commun.* **2014**, *5*, 4055.
- (10) Wang, H.; Zhang, C.; Rana, F. Ultrafast dynamics of defect-assisted electron-hole recombination in monolayer MoS₂. *Nano Lett.* **2015**, *15*, 339–345.
- (11) Ihli, J.; Green, D. C.; Lynch, C.; Holden, M. A.; Lee, P. A.; Zhang, S.; Robinson, I. K.; Webb, S. E. D.; Meldrum, F. C. Super-resolution microscopy reveals shape and distribution of dislocations in single-crystal nanocomposites. *Angew. Chem., Int. Ed.* **2019**, *58*, 17328–17334.
- (12) Srinivasan, R.; Feenstra, J. S.; Park, S. T.; Xu, S.; Zewail, A. H. Dark structures in molecular radiationless transitions determined by ultrafast diffraction. *Science* **2005**, *307*, 558–563.
- (13) Cremons, D. R.; Plemmons, D. A.; Flannigan, D. J. Femtosecond electron imaging of defect-modulated phonon dynamics. *Nat. Commun.* **2016**, *7*, 11230.
- (14) VandenBussche, E. J.; Flannigan, D. J. High-resolution analogue of time-domain phonon spectroscopy in the transmission electron microscope. *Philos. Trans. R. Soc., A* **2020**, *378*, 20190598.
- (15) Cremons, D. R.; Plemmons, D. A.; Flannigan, D. J. Defect-mediated phonon dynamics in TaS₂ and WSe₂. *Struct. Dyn.* **2017**, *4*, 044019.
- (16) Reisbick, S. A.; Zhang, Y.; Chen, J.; Engen, P. E.; Flannigan, D. J. Coherent phonon disruption and lock-in during a photoinduced charge-density-wave phase transition. *J. Phys. Chem. Lett.* **2021**, *12*, 6439–6447.
- (17) Hui, Y. Y.; Liu, X.; Jie, W.; Chan, N. Y.; Hao, J.; Hsu, Y.-T.; Li, L.-J.; Guo, W.; Lau, S. P. Exceptional tunability of band energy in a compressively strained trilayer MoS₂ sheet. *ACS Nano* **2013**, *7*, 7126–7131.
- (18) Zhang, Y.; Flannigan, D. J. Observation of anisotropic strain-wave dynamics and few-layer dephasing in MoS₂ with ultrafast electron microscopy. *Nano Lett.* **2019**, *19*, 8216–8224.
- (19) Aboalazadeh, Z.; Sudak, L. J.; Egberts, P. Nanoscale spatial mapping of mechanical properties through dynamic atomic force microscopy. *Beilstein J. Nanotechnol.* **2019**, *10*, 1332–1347.

- (20) Zewail, A. H. Four-dimensional electron microscopy. *Science* **2010**, 328, 187–193.
- (21) Flannigan, D. J.; Zewail, A. H. 4D electron microscopy: Principles and applications. *Acc. Chem. Res.* **2012**, 45, 1828–1839.
- (22) Plemmons, D. A.; Suri, P. K.; Flannigan, D. J. Probing structural and electronic dynamics with ultrafast electron microscopy. *Chem. Mater.* **2015**, 27, 3178–3192.
- (23) Kwon, O.-H.; Barwick, B.; Park, H. S.; Baskin, J. S.; Zewail, A. H. Nanoscale mechanical drumming visualized by 4D electron microscopy. *Nano Lett.* **2008**, 8, 3557–3562.
- (24) Du, D. X.; Flannigan, D. J. Imaging phonon dynamics with ultrafast electron microscopy: Kinematical and dynamical simulations. *Struct. Dyn.* **2020**, 7, 024103.
- (25) Cremons, D. R.; Du, D. X.; Flannigan, D. J. Picosecond phase-velocity dispersion of hypersonic phonons imaged with ultrafast electron microscopy. *Phys. Rev. Mater.* **2017**, 1, 073801.
- (26) Feldman, J. L. Elastic constants of 2H-MoS₂ and 2H-NbSe₂ extracted from measured dispersion curves and linear compressibilities. *J. Phys. Chem. Solids* **1976**, 37, 1141–1144.
- (27) Mannebach, E. M.; et al. Dynamic optical tuning of interlayer interactions in the transition metal dichalcogenides. *Nano Lett.* **2017**, 17, 7761–7766.
- (28) Mannebach, E. M.; et al. Dynamic structural response and deformations of monolayer MoS₂ visualized by femtosecond electron diffraction. *Nano Lett.* **2015**, 15, 6889–6895.
- (29) Völzer, T.; Lütgens, M.; Fennel, F.; Lochbrunner, S. Recombination dynamics of optically excited charge carriers in bulk MoS₂. *J. Phys. B: At., Mol. Opt. Phys.* **2017**, 50, 194003.
- (30) Komiyama, M.; Tomita, H.; Yoda, E. Electronic “edge” state on molybdenite basal plane observed by ultrahigh-vacuum scanning tunneling microscopy and spectroscopy. *Jpn. J. Appl. Phys.* **2007**, 46, 5964–5969.
- (31) Da Silva, J. L. F.; Schroeder, K.; Blügel, S. Linear scaling of the interlayer relaxations of the vicinal Cu(*p,p,p*-2) surfaces with the number of atom-rows in the terraces. *Surf. Sci.* **2006**, 600, 3008–3014.
- (32) Tripathi, M.; et al. Structural defects modulate electronic and nanomechanical properties of 2D materials. *ACS Nano* **2021**, 15, 2520–2531.
- (33) Liu, K.; Zhang, L.; Cao, T.; Jin, C.; Qiu, D.; Zhou, Q.; Zettl, A.; Yang, P.; Louie, S. G.; Wang, F. Evolution of interlayer coupling in twisted molybdenum disulfide bilayers. *Nat. Commun.* **2014**, 5, 4966.
- (34) Wang, G.; Dai, Z.; Xiao, J.; Feng, S.; Weng, C.; Liu, L.; Xu, Z.; Huang, R.; Zhang, Z. Bending of multilayer van der Waals materials. *Phys. Rev. Lett.* **2019**, 123, 116101.
- (35) Heid, R.; Bohnen, K. P.; Kara, A.; Rahman, T. S. *Ab initio* calculations of multilayer relaxations of stepped Cu surfaces. *Phys. Rev. B: Condens. Matter Mater. Phys.* **2002**, 65, 115405.
- (36) Han, E.; et al. Ultrasoft slip-mediated bending in few-layer graphene. *Nat. Mater.* **2020**, 19, 305–309.
- (37) Shen, Y.; Wu, H. Interlayer shear effect on multilayer graphene subjected to bending. *Appl. Phys. Lett.* **2012**, 100, 101909.
- (38) Reisbick, S. A.; Zhang, Y.; Flannigan, D. J. Influence of discrete defects on observed acoustic-phonon dynamics in layered materials probed with ultrafast electron microscopy. *J. Phys. Chem. A* **2020**, 124, 1877–1884.
- (39) Conley, H. J.; Wang, B.; Ziegler, J. I.; Haglund, R. F., Jr.; Pantelides, S. T.; Bolotin, K. I. Bandgap engineering of strained monolayer and bilayer MoS₂. *Nano Lett.* **2013**, 13, 3626–3630.
- (40) Huang, M.; Yan, H.; Chen, C.; Song, D.; Heinz, T. F.; Hone, J. Phonon softening and crystallographic orientation of strained graphene studied by Raman spectroscopy. *Proc. Natl. Acad. Sci. U. S. A.* **2009**, 106, 7304–7308.
- (41) Kieft, E.; Schliep, K. B.; Suri, P. K.; Flannigan, D. J. Communication: Effects of thermionic-gun parameters on operating modes in ultrafast electron microscopy. *Struct. Dyn.* **2015**, 2, 051101.
- (42) Plemmons, D. A.; Flannigan, D. J. Ultrafast electron microscopy: Instrument response from the single-electron to high bunch-charge regimes. *Chem. Phys. Lett.* **2017**, 683, 186–192.
- (43) Du, D. X.; Reisbick, S. A.; Flannigan, D. J. UEMtomaton: A source-available platform to aid in start-up of ultrafast electron microscopy labs. *Ultramicroscopy* **2021**, 223, 113235.
- (44) Schindelin, J.; et al. Fiji: An open-source platform for biological-image analysis. *Nat. Methods* **2012**, 9, 676–682.
- (45) Schneider, C. A.; Rasband, W. S.; Eliceiri, K. W. NIH Image to ImageJ: 25 years of image analysis. *Nat. Methods* **2012**, 9, 671–675.